Neutrophils in nasal polyps exhibit transcriptional adaptation and proinflammatory role depend on local polyp milieu

Chen Zhang[1,2*], Qianqian Zhang[1*], Jiani Chen[1], Han Li[1], Fuying Cheng[1], Yizhang Wang[1], Yingqi Gao[1], Yumin Zhou[1], Le Shi[1], Yufei Yang[1], Juan Liu[1], Kai Xue[1], Yaguang Zhang[3], Hongmeng Yu[1], Dehui Wang[1], Li Hu[1**], Huan Wang[1**], Xicai Sun[1,2**]

[1] ENT Institute and Department of Otorhinolaryngology, Eye & ENT Hospital, Fudan University, Shanghai, China; High Altitude Rhinology Research Center of Eye & ENT Hospital of Fudan University and People's Hospital of Shigatse City, China

[2] Department of Otolaryngology, People's Hospital of Shigatse City, Shigatse, China

[3] Med-X Institute, Center for Immunological and Metabolic Diseases, The First Affiliated Hospital of Xi'an JiaoTong University, Xi'an JiaoTong University, Xi'an, Shaanxi, P. R. China

[*] These authors contributed equally to this work.

Corresponding author:

[**] Correspondence:

[**] Xicai Sun, Eye & ENT Hospital, Fudan University, 83 Fenyang Road, Shanghai 200031, China; High Altitude Rhinology Research Center of Eye & ENT Hospital of Fudan University and People's Hospital of Shigatse City, China; Department of Otolaryngology, People's Hospital of Shigatse City, Shigatse, China; Tel: 021-64377134; e-mail: laryngeal@163.com.

[**] Huan Wang, Eye & ENT Hospital, Fudan University, 83 Fenyang Road, Shanghai

200031, China; Tel: 021-64377134; e-mail: huanwang14@fudan.edu.cn.

** Li Hu, Eye & ENT Hospital, Fudan University, 83 Fenyang Road, Shanghai 200031, China; Tel: 021-64377134; e-mail: hl318ent@163.com.

Abstract

Chronic rhinosinusitis with nasal polyps (CRSwNP) is an inflammatory upper airway disease, divided into eosinophilic CRSwNP (eCRSwNP) and noneosinophilic CRSwNP (neCRSwNP) according to eosinophilic levels. Neutrophils are major effector cells in CRSwNP. but their role in different inflammatory environments remain largely unclear. We performed an integrated transcriptome analysis of polyp-infiltrating neutrophils from CRSwNP patients, using healthy donor blood as a control. Additional experiments including flow cytometry and in vitro epithelial cells as well as fibroblasts culture were performed to evaluate the phenotypic feature and functional role of neutrophils in CRSwNP. The scRNA-sequencing analysis demonstrated that neutrophils were classified into five functional subsets, with GBP5+ neutrophils occurring mainly in neCRSwNPs and a high proportion of CXCL8+ neutrophils in both subendotypes. GBP5+ neutrophils exhibited significant IFN-I pathway activity in neCRSwNPs. CXCL8+ neutrophils displayed increased neutrophil activation scores and mainly secrete Oncostatin M (OSM), which facilitates communication with other cells. In vitro experiments showed that OSM enhances IL-13- or IL-17-mediated immune responses in nasal epithelial cells and fibroblasts. Our findings indicate that neutrophils display transcriptional plasticity and activation when exposed to polyp tissue, contributing to CRSwNP pathogenesis by releasing OSM, which interacts with epithelial cells and fibroblasts depending on the

inflammatory environment.

Keywords:

Nasal polyps; Neutrophil heterogeneity; Single-cell RNA sequencing; Oncostatin M; Type 2 inflammation.

Introduction

Chronic rhinosinusitis with nasal polyp (CRSwNP) is a common disease characterized by chronic mucosal inflammation in the upper airway and generally classified as eosinophilic CRSwNP (eCRSwNP) or noneosinophilic CRSwNP (neCRSwNP) based on the eosinophilic status of the polyp tissue(1, 2). CRSwNP patients in Western countries are characterized mainly by type 2 inflammation, with increased eosinophil infiltration and elevated type 2 cytokines. Although the proportion of eCRSwNP in Asian CRSwNP patients has increased in recent years, neCRSwNP still accounts for a relatively high percentage (30%-50%) and is associated with mixed inflammation, including type 1 (IFN-γ) and/or type 3 (IL-17) immune responses(3-5).

Early studies demonstrated prominent neutrophilic inflammation in neCRSwNP patients, whereas accumulating evidence observed increased infiltration of neutrophils in eCRSwNP patients(6). Moreover, the concurrent increase in neutrophil infiltration in eCRSwNP patients is associated with worse quality of life, greater symptom burden, and greater refractoriness(7, 8). A recent study revealed that neutrophil extracellular traps are abundant near epithelial cells in nasal polyps (NPs) and can induce epithelial basal cell hyperplasia and possibly further polyp formation(9). Additionally, neutrophils in neCRSwNP patients may contribute to tissue fibrosis via TGF-β2 production(10). Despite these findings, the

role of neutrophil infiltration in the CRSwNP pathogenesis remains largely unknown. In particular, the phenotype and functional difference of neutrophils under distinct inflammatory milieu of CRSwNP have not been compared.

Single-cell RNA sequencing (scRNA-sequencing) has emerged as a powerful tool for determining the functional status and heterogeneity of various cells. Although technical difficulties exist in isolating and preserving neutrophils, a few groups have recently applied scRNA-sequencing to examine the phenotypic and functional heterogeneity of blood and tissue neutrophils in healthy and diseased states(11-14). A systematic analysis of the transcriptomic features of neutrophils from eCRSwNP and neCRSwNP patients is essential for understanding neutrophil plasticity and improving CRSwNP treatment. Here, we firstly performed an integrated transcriptome analysis of CRSwNP neutrophils at the single-cell level to assess the activation status and transcriptome heterogeneity of polyp-infiltrating neutrophils in different inflammatory backgrounds.

Results

The scRNA-sequencing profiling maps of neutrophils in nasal polyps

We constructed a single-cell transcriptome atlas via the integrated analysis and batch effect removal of 22 patient specimens from the Gene Expression Omnibus (GEO) and Genome Sequence Archive (GSA) databases, along with our own sequencing data (Figure 1A, Supplemental Figure 1, A and B). We annotated eight cell types within distinct clusters according to cell type-specific gene markers (Figure 1, B and C, Supplemental Figure 1C, Supplemental Table 6).

To assess the role of neutrophils in CRSwNP, 9,735 neutrophils were further analyzed

(Figure 1D). We explored neutrophil differentiation trajectory, revealing a unidirectional trajectory from peripheral blood (PB) to locally infiltrated neutrophils (Figure 1E, Supplemental Table 7). Pseudotime heatmap analysis showed heightened expression of genes linked to neutrophil activation (CXCL8 and IL1B) and interferon pathways (GBP5 and IGS15) during later differentiation stages (Figure 1F), indicating functional changes as neutrophils progressed.

Next, we performed differentially expressed genes (DEGs) and functional analyses of neutrophils between CRSwNP and PB (Figure 1, G and I, Supplemental Table 8-9). With Molecular Complex Detection (MCODE) applied for module analysis in the protein–protein interaction (PPI) network, all nodes were classified and colored according to their function. The most compact MCODE module, comprising genes upregulated in both neCRSwNP and eCRSwNP neutrophils compared to PB neutrophils, primarily involved inflammatory and cytokine pathway response (Figure 1, H and J). Functional and pathway analyses revealed enrichment of cytokine-mediated signaling and response to LPS in both neCRSwNP and eCRSwNP neutrophils (Supplemental Figure 1,F and G, Supplemental Table 10-15).

Neutrophils are activated in both eCRSwNPs and neCRSwNPs

Neutrophil activation was previously demonstrated by bulk transcriptome sequencing in CRSwNP patients from Western countries(6). Similarly, our scRNA-sequencing analysis revealed that the neutrophil activation (GO:0042119) score was significantly greater in the eCRSwNP group than the PB group (Figure 2A, $p < 0.001$). Additionally, the neCRSwNP group exhibited a greater activation score than both the PB and eCRSwNP groups ($p < 0.001$). Notably, in neCRSwNP and eCRSwNP neutrophils, key activated molecules, such

as CXCL1, CXCL8, CD44, PLAUR, NFKB1, FTH1, TNFAIP6, and IL1RN were upregulated (Figure 2A)(6, 15). In addition, the inflammasome pathway signature score was elevated in neCRSwNP and eCRSwNP neutrophils, indicating the activation of innate inflammatory responses (Figure 2B). Our DEG analysis also revealed increased expression of elements in both canonical and noncanonical inflammasome pathway (Figure 2C).

We next confirmed the increased accumulation of neutrophils in both neCRSwNP and eCRSwNP by Immunohistochemistry and ELISA for neutrophil elastase (NE) (Figure 2, D and E). To further validate the activation status of neutrophils in NPs, we used flow cytometry to assess the cell surface expression of CD62L, a marker of neutrophil activation.(6, 16) (Figure 2, F and G, Supplemental Figure 2B). Consistent with a prior study, we also detected a decrease in CD62L expression on NP neutrophils ($p < 0.001$, Figure 1H). Furthermore, we observed an increase in the CD62L-negative cell population in eCRSwNP neutrophils compared to that in PB neutrophils ($p < 0.01$), with a more pronounced increase in neCRSwNP neutrophils than in both eCRSwNP and PB neutrophils ($p < 0.001$, Figure 1I). Collectively, our findings indicated that neutrophils are activated and serve a proinflammatory role in CRSwNPs.

Neutrophils in nasal polyps consist of distinct transcriptional subsets

Recent studies have demonstrated that human neutrophils exist in distinct transcriptional states and exhibit heterogeneity(12, 13). We partitioned neutrophils into 10 clusters based on DEGs and calculated the ratio of observed to expected cell numbers (Ro/e) (Figure 3, A and B, Supplemental Table 16). Cluster 9 was excluded because it predominantly expressed the eosinophil marker CLC for further analysis (Figure 3C)(17). Considering previous grouping strategies, five distinct transcriptional subsets of neutrophils were identified:

S100A8+, GBP5+, CXCL8+, EPHB1+, and S100A12+ neutrophils (Figure 3D, Supplemental Table 17).

We assessed neutrophil tissue enrichment using Ro/e analysis (Figure 3, E and F). S100A8+, EPHB1+, and S100A12+ neutrophils were preferentially enriched among PB neutrophils, while CXCL8+ neutrophils were enriched in both neCRSwNP and eCRSwNP neutrophils. S100A8+ and S100A12+ neutrophils exhibited upregulation of S100 family members (S100A4, S100A6, and S100A8), MME and LST1, which are associated with the maturation state of neutrophils(18). EPHB1+ neutrophils were more prevalent among PB neutrophils whose expression of upregulated genes (IGF1R and EGR1) increased in response to insulin stimulation. CXCL8+ neutrophils displayed upregulated expression of neutrophil activation-associated genes (CXCL8, IL1B, and CD83) and senescence-associated genes (G0S2 and CCL3L1). In parallel, we observed greater neutrophil activation and senescence scores for the CXCL8+ subset (Figure 3,G-I). Pathway analysis revealed that the upregulated genes in CXCL8+ neutrophils were significantly associated with cytokine-mediated immune regulation. Therefore, CXCL8+ neutrophils represent activated states and play a proinflammatory role in CRSwNP.

We observed a higher proportion of GBP5+ neutrophils in neCRSwNPs, which displayed elevated expression of interferon-inducible genes, including ISG15, IFIT1, IFIT2, MX1, and GBP5 (Figure 3, F and G). Consistent with a recent report, GBP5+ neutrophils showed increased PD-L1 (CD274) expression with a potential immunosuppressive effect(11) (Supplemental Figure 3A). The response to IFN-I pathway (GO:0034340) was enriched in GBP5+ neutrophils (Figure 3, J and K). Transcription factor analysis further showed increased interferon regulatory factor (IRF) and signal transducer and activator of

transcription (STAT) in GBP5+ neutrophils (Supplemental Figure 3B, Supplemental Table 18). MX1, as an IFN-I-regulated signature gene(19), positively associated with the response to IFN-I pathway (R=0.64; Figure 3L) and displayed significantly higher mRNA expression in neCRSwNPs than normal controls ($p < 0.05$, Figure 3, L and M), indicating IFN-I pathway activity in neCRSwNPs.

Context-specific transcriptional features of neutrophil subsets in eCRSwNP and neCRSwNP

To further investigate the transcriptional differences of individual neutrophil subsets under distinct inflammatory backgrounds, we analyzed the DEGs in each subset (Figure 4A, Supplemental Table 19-23). BFIFA1, encoding SPLUNC1, an antimicrobial protein, was mainly upregulated in the S100A8+, S100A12+, and CXCL8+ subsets in neCRSwNP. Additionally, CXCL8+ neutrophils from neCRSwNP patients exhibited upregulated expression of interferon-induced genes (GBP5, GBP1, and IRF1). S100A8+ and S100A12+ neutrophils in eCRSwNP patients overexpressed genes associated with neutrophil activation (ERG1 and TNFAIP3).

Interestingly, we found that CXCL8 receptors (CXCR1 and CXCR2) expression was notably lower in predominantly polyp-infiltrating CXCL8+ neutrophils in eCRSwNP compared to neCRSwNP (Figure 4B). Flow cytometry confirmed decreased CXCR1 and CXCR2 expression on the eCRSwNP neutrophil surface (Figure 4, C and D, Supplemental Figure 4A).

Overall, these results suggest that polyp-infiltrating neutrophils exhibit heterogeneous functional states and are transcriptionally affected by different inflammatory patterns.

OSM secreted by neutrophils is elevated in CRSwNP

To clarify the pathogenic role of neutrophils in both CRSwNP subendotypes, we further screened the DEGs between CRSwNP and PB neutrophils. Eighty-seven genes, including OSM, CXCL8, and IL1B, were uniformly upregulated in both neCRSwNP and eCRSwNP neutrophils (Supplemental Figure 5, A and B). Next, we analyzed biologically relevant communications between neutrophils and other cell types in NPs (Figure 5, A and B, Supplemental Figure 5C-F). Of particular interest was OSM, as the cell type-specific networks of OSM showed that neutrophils were the prominent source of effector secretion, with fibroblasts, epithelial cells, and endothelial cells being the primary targets (Figure 5C). The scRNA-sequencing data revealed neutrophils, especially CXCL8+ neutrophils, as the dominant cell type expressing OSM in NPs (Figure 5, D and E). Furthermore, ELISA analysis demonstrated higher OSM protein levels in polyp homogenates from both neCRSwNP and eCRSwNP (Figure 5F).

There are two types of OSM receptors: type I (gp130/LIFRα complex) and type II (OSMRβ/gp130 complex). OSM receptors, including gp130 (IL6ST), LIFRα (LIFT), and OSMRβ (OSMR), are predominantly expressed in fibroblasts, epithelial cells, and endothelial cells (Figure 5G). A previous study showed that the OSMRβ/gp130 complex, not the gp130/LIFRα complex, is upregulated and mediates OSM responses in NPs(20).The localization of OSMR was confirmed through co-staining of endothelial cells, epithelial cells, and fibroblasts with VWF, E-CAD, and COL1A1, respectively (Figure 5H). Elevated OSMR expression was also detected in neCRSwNP and eCRSwNP (Figure 5I).

Inspired by recent findings that LPS promoted airway inflammation through OSM secretion from macrophages(21), we found a positive correlation between OSM expression

and the LPS pathway response in polyp-infiltrating neutrophils (Figure 5J). Functional enrichment further revealed a significantly higher response to LPS pathway in neCRSwNP or eCRSwNP neutrophils (Figure 5K).

GM-CSF and G-CSF, inducers of neutrophil differentiation and activation, exhibited elevated protein levels in neCRSwNP and eCRSwNP homogenates compared with those in control uncinate tissues (Figure 5M). GM-CSF also showed a significant positive correlation with OSM (R= 0.31; Figure 5N). To further assess the factors driving neutrophils to produce OSM, we treated PB neutrophils with LPS, G-CSF, and GM-CSF. Results suggested that LPS stimulated OSM expression and synergized with GM-CSF to enhance OSM production (Figure 5O).

OSM modulates pathogenic pathways in epithelial cells and fibroblasts depending on inflammatory milieu

Consistent with previous reports, NE expression did not significantly correlate with eosinophil marker (ECP) expression in NP homogenates(6). However, we found that neutrophil-derived OSM expression was significantly positively correlated with ECP expression (R= 0.35; Figure 6A), which suggest the potential role of neutrophils in promoting eosinophilic inflammation in NPs. To further elucidate the OSM-regulated pathogenic pathway in eCRSwNP, we performed enrichment analysis of genes upregulated in OSM-targeted epithelial cells and fibroblasts. The scRNA-sequencing data revealed increased IL-13 signaling pathway scores in eCRSwNP epithelial cells and fibroblasts (Figure 6B). Additionally, downstream inflammatory factors of the IL-13 signaling pathway, such as CCL26 and periostin, were significantly increased in eCRSwNP polyp homogenates and mainly produced by fibroblasts and epithelial cells (Figure 6, C and D).

We speculated that OSM may affect targeting cells by modulating the IL-13 immune response. Subsequently, we found that OSM significantly enhanced IL-13-dependent CCL26 and periostin production in fibroblasts but not in epithelial cells (Figure 6, E and F). To explore the underlying mechanism, we examined IL-13 receptor distributions and alterations following OSM stimulation. Interestingly, OSM significantly promoted IL4R and IL13RA2 expression in fibroblasts (Figure 6G). The scRNA-sequencing data also showed a significant positive correlation between IL4R expression levels in fibroblasts and OSM expression levels in NPs (Figure 6G). These results suggest that neutrophils in eCRSwNPs may amplify eosinophilic inflammation by regulating the IL-13-mediated immune response in fibroblasts.

Neutrophils are the main effector cells in neCRSwNP patients, and our previous work suggested prominent type 3 inflammation in our neCRSwNP cohort(22). We next sought to determine the regulatory role of OSM in neCRSwNP. We observed a positive correlation between OSM and NE, IL-17A, G-CSF, IL-6, and IL-8 in tissue homogenates (Figure 6H). A set of IL-17-responsive genes was commonly upregulated in epithelial cells, fibroblasts, and endothelial cells in neCRSwNP (Figure 6I). The pivotal downstream chemokines of IL-17, such as G-CSF, are predominantly expressed in epithelial cells. IL-8 was also expressed in epithelial cells and fibroblasts (Figure 6J). To investigate the modulatory effect of OSM on the type 3 inflammatory milieu, we utilized IL-17A in combination with OSM to stimulate fibroblasts and human nasal epithelial cells (HNECs). We found robust upregulation of G-CSF and IL-8 upon co-stimulation compared to IL-17A stimulation alone (Figure 6, K and L, Supplemental Figure 6E-H), suggesting neutrophils in neCRSwNP could intensify neutrophilic inflammation by releasing OSM, thereby

enhancing the proinflammatory effect of IL-17A. However, this modulatory effect was not related to IL-17 receptors because their expression did not change after OSM stimulation (Supplemental Figure 6I). Nevertheless, OSM stimulation significantly upregulated NF-κB inhibitor-ζ (IκBζ) expression, a crucial mediator of IL-17A signaling pathway in psoriasis(23), thereby possibly providing an additive effect on IL-17A effect in HNECs and fibroblasts (Supplemental Figure 6J).

As mentioned above, eCRSwNP and neCRSwNP patients exhibited consistently upregulated OSM expression and cellular sources from CXCL8+ neutrophils, suggesting that neutrophil-derived OSM specifically strengthens inflammation according to the tissue microenvironment.

Discussion

It is well documented that infiltrated neutrophils serve as the main effector cells in CRSwNP patients with non-type 2 inflammation. The presence of neutrophils, as well as their activation status in type 2 CRSwNP, has also been observed in recent studies(6, 7, 24). However, comparisons of the functional status of neutrophils within different inflammatory backgrounds have not yet been performed. Our study is the first to utilize scRNA-sequencing to determine neutrophils functional diversity in NPs. We demonstrated activated neutrophils in both eCRSwNPs and neCRSwNPs based on scRNA-sequencing and CD62L flow cytometry. Given recent findings that neutrophils are highly heterogeneous, in contrast with the traditional view that neutrophils are a homogeneous antimicrobial cell population, we hypothesized and confirmed that polyp-infiltrating neutrophils are composed of five functional subsets with distinct markers and that CXCL8+ and GBP5+ neutrophil subsets account for a greater proportion of polyp-infiltrating

neutrophils than blood neutrophils. We also provide the first evidence that transcriptomic modulation occurs in neutrophils after they migrate to NPs and that tissue-specific transcriptional regulation occurs in two CRSwNP endotypes. Furthermore, we found that the proinflammatory effect of CXCL8+ neutrophil-derived OSM on epithelial cells and fibroblasts was dependent on the tissue inflammatory microenvironment of CRSwNPs.

Consistent with previous work, we observed a comparable and elevated number of infiltrated neutrophils in both eCRSwNP and neCRSwNP(24). We also confirmed highly activated neutrophils in eCRSwNPs with lower CD62L expression, as detected by flow cytometry(6, 25). Although neutrophils have been conventionally considered as the main effector cells in neCRSwNP, we confirmed their activation status by decreasing the cell surface expression of CD62L. Recently, the Northwestern group performed bulk RNA sequencing of sorted neutrophils from NPs and blood, confirmed the infiltrated neutrophil activation in NPs by GO analysis(6). In the present study, we analyzed neutrophils from polyp tissue of both subtypes using scRNA-sequencing. Interestingly, the GO analysis of upregulated genes also demonstrated the activation of neutrophils in both CRSwNP subtypes. Moreover, we also observed a significant increase of IL1B expression in neutrophils from both CRSwNP subtypes. Inflammasome activation with increased IL-1β expression has been reported previously in eCRSwNPs and neCRSwNPs, associated with neutrophilic inflammation(26-28). Our scRNA-sequencing analysis indicated increased expression of inflammasome-related genes, such as GSDMD, NLRP3, and AIM2. Together, these findings indicate that activated neutrophils may contribute to the pathogenesis of both CRSwNP subtypes through activating inflammasome pathways.

The five established neutrophil subsets were conserved between PB and NPs, with

CXCL8+ and GBP5+ neutrophils presenting higher activation and aging scores. Prior studies reported that tissue-infiltrating neutrophils aged and became more active(29, 30). Interestingly, the CXCL8+ neutrophils were more abundant in NPs from both subendotypes, confirming that the migration of neutrophils into polyps was transcriptionally activated. Particularly, the proportion of the GBP5+ neutrophils in neCRSwNP was significantly greater than that in eCRSwNP, and the CXCL8+ neutrophils in neCRSwNP patients also presented with elevated expression of interferon-induced genes. Moreover, elevated expression of MX1, which has been previously evaluated as a biomarker for predicting type I interferon activity, was observed in neCRSwNP(19). Taken together, these findings indicated the activation of type I IFN signaling in neCRSwNP. Traditionally, type I interferon activation is associated with protection from viral or bacterial infections and contributes to the perpetuation of inflammation in several autoimmune diseases(31-33). The molecular basis driving the activation of type I interferon in neutrophils from neCRSwNP, as well as its pathogenic role, remains to be elucidated.

Increased neutrophil infiltration was associated with steroid unresponsiveness in CRSwNP patients(34, 35). Elevated CCL4L2 expression in neutrophils was associated with inhaled corticosteroids in patients with asthma(36). Our present study revealed increased expression of CCL4L2 in eCRSwNP neutrophils, indicating the refractoriness of steroid treatment in severe CRSwNP patients with mixed inflammation (Supplemental Figure 2A). Moreover, several neutrophil subsets from eCRSwNP displayed decreased expression of CXCR1 and CXCR2 in comparison to those from neCRSwNP. A recent study reported the downregulatory effect of IL-4 or IL-13 on CXCR1 and CXCR2, and the decreased

expression of CXCR1 and CXCR2 in eCRSwNP was possibly related to eosinophilic inflammation(37). Neutrophil migration driven by CXCL8 depended on the surface abundance of CXCR1 and CXCR2. Therefore, obvious neutrophil infiltration in eCRSwNP may be induced by other chemotaxis factors(38). These data further demonstrated that neutrophils underwent transcriptome modulation in response to the distinct inflammatory milieu.

The IL-13-mediated immune response serves as a pivotal biological process in the pathogenesis of eCRSwNP, which has been confirmed by the excellent efficacy of dupilumab, which targets IL-4Ra(39). Epithelial cells and fibroblasts are the main effector cells of the IL-13-mediated immune response in eCRSwNP patients(40, 41). Cell communication analysis revealed functional interactions between neutrophils and multiple effector cells, including epithelial cells and fibroblasts(42). Moreover, the OSM-mediated signaling pathway was specific for neutrophil-mediated crosstalk with epithelial cells and fibroblasts. In line with a previous report, OSM was significantly upregulated in eCRSwNPs and located in neutrophils(43). Our scRNA analysis revealed that OSM was mainly produced by CXCL8+ neutrophils. The same group reported that in combination with IL-4, OSM promotes HNECs to release TSLP through upregulating IL-4Ra expression(44). Our work revealed that OSM synergizes with IL-13 to enhance the production of CCL26 and periostin by fibroblasts. Prior findings have demonstrated the critical role of CCL26 and periostin in regulating eosinophilic inflammation(45-47). These findings further supported the concept that neutrophils could significantly amplify type 2 inflammation through releasing OSM.

Previous studies, including our recent report, have demonstrated that elevated IL-17A

levels are associated with CRSwNP and neutrophilic inflammation(22). Additionally, using murine CRSwNP model in which IL-17A is targeted indicates the pathogenic function of IL-17A(48, 49). Despite the equivalent numbers of infiltrated neutrophils and NE levels in eCRSwNP and neCRSwNP, we detected significantly greater IL-17A levels in neCRSwNP. This may imply a prominent pathogenic effect of IL-17A in neCRSwNP. Our study revealed that genes upregulated in multiple effector cells, including epithelial cells, fibroblasts, and endothelial cells, were enriched in the IL-17A-mediated immune response pathway, which further indicated the central role of IL-17A in the pathogenesis of neCRSwNP. OSM has been reported to activate STAT3 signaling in airway smooth muscle cells and enhance IL-6 and CCL2 expression synergistically with IL-17(50, 51). We found equivalently elevated OSM expression in neCRSwNP and detected its communication with epithelial cells and fibroblasts, prompting further investigation into OSM in neCRSwNP. Our further in vitro experiments revealed the ability of OSM to amplify the proinflammatory effect of IL-17A on nasal epithelial cells and fibroblasts. A previous study revealed that IκBζ mediates the synergistic inflammatory response to IL-17 and TNF-alpha in fibroblasts(52). IκBζ expression can be induced through the transcription factor STAT3 or NF-kB(53-55). Collectively, our findings suggested that the synergistic effect of OSM may involve increased IκBζ expression mediated by STAT3 activation.

While our study provided a novel understanding of the functional versatility and heterogeneity of NP neutrophils, it has several limitations. First, our cohort did not employ scRNA-sequencing to compare neutrophils from normal sinonasal tissue to NP neutrophils, as insufficient neutrophils from normal tissue could be obtained. Second, we did not analyze circulating neutrophils from CRSwNP. Although recent bulk sequencing analysis

did not reveal activation of CRSwNP PB neutrophils in comparison to control PB neutrophils, the phenotypic and transcriptomic features of PB neutrophils in CRSwNP deserve future clarification(6). Finally, we focused primarily on the transcriptomic features of NP neutrophils and complemented the analysis with flow cytometry and in vitro validation. Further studies combining mass cytometry and epigenomic approaches will fully define the phenotypic and functional features of polyp-infiltrating neutrophils.

Conclusions

In conclusion, our study demonstrated that neutrophils are highly heterogeneous, with five functional subsets and acquired transcriptional adaptation when exposed to a polyp tissue environment. While neutrophils from both eCRSwNP and neCRSwNP have several overlapping functional features, we also observed context-specific transcriptional profiling. Furthermore, we revealed that neutrophils perform a modulatory role in the pathogenesis of CRSwNP by releasing OSM to interact with epithelial cells and fibroblasts and then amplifying eosinophilic or neutrophilic inflammation in a manner dependent on the inflammatory environment.

Methods

Sex as a biological variable.

Our study included both male and female patients.

Clinical samples

All subjects, including CRSwNP patients and controls, were recruited from the Department

of Otorhinolaryngology at the Eye and ENT Hospital of Fudan University. CRSwNP was diagnosed based on the criteria defined by recently released European and American guidelines(1, 2). Subjects with an isolated antrochoanal polyp, fungal rhinosinusitis, cystic fibrosis, or unilateral NP were excluded from the study. No subjects used antibiotics or topical/oral corticosteroids for at least 1 month before the operation. The clinical characteristics of each patient, including age, sex, history of smoking, prior sinus surgery history, asthma status, and CT score, were collected and are listed in Supplemental Table 1. The Lund-Mackay staging score, maxillary sinus score, ethmoid sinus score, and E/M ratio (the ratio of the ethmoid and maxillary sinus scores) were assessed by one independent radiologist(56). ECRSwNP was defined as tissue eosinophils above or equal to 10/high-power field (HPF) according to hematoxylin and eosin staining, whereas neCRSwNP was defined as the absence of evidence of eosinophilia(1, 22, 57). Polyp specimens were collected from CRSwNP patients who failed conservative medical therapy and underwent endoscopic sinus surgery. Patients who underwent endoscopic orbital decompression, cerebral spinal fluid leakage repair, or skull base surgery without a clinical or radiographic history of CRS, allergic rhinitis, or asthma were included as control subjects. Uncinate tissue (UT) was obtained from control subjects for subsequent biological analysis.

Single-cell RNA sequencing data

The original FASTQ file data of nasal polyp tissues (5 neCRSwNP and 6 eCRSwNP samples) were retrieved from the GSA under accession number HRA000772(57). Additionally, five PB samples from healthy controls were obtained from the GEO under accession number GSE157789(58). These datasets were then integrated with our

sequencing data from six polyp tissues. In total, our analysis included 22 samples, consisting of 5 PB samples, 7 neCRSwNP samples, and 10 eCRSwNP samples (Figure 1A).

Preparation of single-cell suspensions

Polyp tissue samples (2 neCRSwNPs, 4 eCRSwNPs) were collected in MACS tissue storage solution (130-100-008, Miltenyi Biotec, Germany) within 30 min of the surgical procedure. Then, the samples were dissociated into single-cell suspensions by mechanical dissociation for 30 minutes with a gentleMACS™ Dissociator (130-093-235, Miltenyi Biotec, Germany), with 1 mg/mL collagenase I (Sigma–Aldrich, USA), and 30 μg/mL DNase I (Sigma–Aldrich, USA). The suspension was subsequently centrifuged at 300 × g for 5 min at 4 °C, after which the single-cell suspension was filtered through a 40-μm nylon cell strainer (Falcon). Red blood cell lysis solution (Sigma–Aldrich, USA) was further used to remove erythrocytes. A Dead Cell Removal Kit (Miltenyi Biotec, Germany) was utilized to remove dead cells, ensuring cell viability > 90%.

Following the manufacturer's protocol, libraries were prepared for scRNA-sequencing using the Chromium Next GEM Single Cell 3′ Reagent Kit v3.1 (10X Genomics, USA). Briefly, single-cell suspensions were loaded onto a Chromium Single-Cell Controller Instrument (10X Genomics, USA) to generate single-cell gel beads in emulsions (GEMs). After GEM generation, reverse transcription reactions were carried out to produce full-length barcode cDNA, followed by the disruption of emulsions using the recovery agent. Barcoded cDNA was subsequently purified with DynaBeads Myone Silane Beads (Thermo Fisher Scientific, USA) and amplified by PCR with cycles adjusted based on the cell recovery rate. The amplified cDNA was then fragmented, end-repaired, A-tailed, index adapter-ligated, and used for library amplification. Library sequencing was performed on

the Illumina sequencing platform (HiSeq X Ten; Illumina, USA), and 150 bp paired-end reads were generated. Then, we obtained the original FASTQ file data.

Single-cell RNA sequencing data preprocessing and quality control

To process the data, we used the Cell Ranger software pipeline (version 6.1.2) provided by 10× Genomics. This pipeline allowed us to demultiplex cellular barcodes, map reads to the genome and transcriptome using the STAR aligner, and downsample reads as necessary to generate normalized aggregate data across samples. This process yielded a matrix of gene counts associated with individual cells.

To capture neutrophils in the raw data, we used the 'cellranger count' command with the 'force-cells' option to include low-UMI barcodes and the 'include-introns' option to accommodate increased intron retention in neutrophils, as advised in the 10X Genomics official guide(59). We processed the unique molecular identifier (UMI) count matrix using the R package Seurat (version 4.0.3)(60). To accurately capture neutrophils while eliminating low-quality cells, a significant concern in microdroplet-based experiments, we applied the following criteria: (1) genes expressed in fewer than 3 cells were filtered out; (2) the number of detected genes was above 100; and (3) the percentage of mitochondrial genes was less than 50. To mitigate unexpected noise and expression artifacts, genes associated with mitochondria and ribosomes were excluded (Supplemental Figure 1A, Supplemental Table 2).

After applying these quality control criteria, the downstream analyses included 200,091 single cells with 31,215 genes. To obtain the normalized count, library size normalization was performed with the NormalizeData function in Seurat(61). Specifically, the datasets were normalized, multiplied by a scaling factor, and log-transformed using the

LogNormalize function. After rescaling the integrated object, graph-based clustering was performed to cluster cells according to their gene expression profile using the FindClusters function, and uniform manifold approximation and projection (UMAP) and 2-dimensional t-distributed stochastic neighbor embedding (tSNE) calculations were performed(62). To merge samples and remove batch effects, we applied Harmony with default parameters to the first 30 principal components (PCs) to obtain the corrected PC embeddings(63). Then, UMAP and tSNE were generated again based on the Harmony Reduction (Supplemental Figure 1B)(63). Clustering (resolution: 0.3) was determined by evaluating cluster stability using the Clustree package(64). Finally, cell types were identified based on prior articles and reference transcriptomic datasets, such as the Human Primary Cell Atlas (Supplemental Table 3, Supplemental Figure 1C)(22, 65, 66).

Analytical strategies for neutrophils

The subset of neutrophils was selected for further analysis. Harmony and Seurat were used for removing batch effects, dimension reduction, clustering, and differential gene expression. A resolution parameter of 0.8 was used for clustering. To annotate cell clusters, the DEGs for each cell cluster were identified by comparing each cluster to all other clusters using the FindAllMarkers function.

Tissue distribution of clusters

We compared the ratio of observed to expected cell numbers (Ro/e) in different tissues to quantify the tissue preference of each cluster using the epitools R package(67). One cluster was identified as enriched in a specific tissue if Ro/e > 1.

Pseudotime analysis

We determined the developmental pseudotime of neutrophils with the Monocle2 package(68). Initially, the data matrix was converted from the Seurat object to the CellDataSet object using the new CellDataSet function. We used the differentialGeneTest function package to select ordering genes with a q value < 0.01, which is likely to be informative for ordering cells along the pseudotime trajectory. Dimensional reduction clustering analysis was performed with the reduceDimension function, followed by trajectory inference with the orderCells function. The top 60 genes that changed as a function of pseudotime were identified and visualized using the plot_pseudotime_heatmap function.

Differentially expressed genes and protein–protein interaction analysis

DEGs were identified using Seurat's FindMarkers function and the MAST test. The criteria for significance were set at a P value < 0.05 and a fold change (FC) ≥ |2|. Volcano plots were generated using the EnhancedVolcano package. For an in-depth exploration of the interactions between these DEGs, we conducted a PPI analysis based on the STRING database(69). To further identify subnetworks of DEGs, we utilized MCODE plugin to screen modules of the PPI network. The results were visualized with Cytoscape (version 3.10.0)(70).

Functional enrichment and gene set enrichment analysis

Gene Ontology (GO) enrichment, Kyoto Encyclopedia of Genes and Genomes (KEGG) pathway enrichment, and gene set enrichment analysis (GSEA) of DEGs were performed

using the clusterProfiler package(71). The results were visualized by the clusterProfiler and GseaVis packages. Next, we calculated the enrichment of multiple genes across different cell clusters and calculated the gene set signature scores utilizing Seurat's AddModuleScore function and the irGSEA package. We obtained gene sets characterizing the response to type I interferon (GO:0034340) and neutrophil activation (GO:0042119) from the Gene Ontology (GO) database. We predicted senescence-associated pathways through published gene sets(72).

Transcription factor analysis

Transcription factor (TF) activity was calculated using the VIPER (version: 1.32.0) and DoRothEA (version: 1.10.0) packages(73, 74). The TF activity was calculated separately for individual cells within each section using regulons with confidence intervals A, B, and C. Then, the estimated enrichment score was calculated based on the z score of the DEGs and was normalized for hierarchical clustering.

Cellular crosstalk

To assess the cellular crosstalk in polyp tissues, we divided the subsets of the neCRSwNP and eCRSwNP groups for further analysis. Following dimension reduction, clustering, and cell type annotation, we quantified cellular crosstalk with the CellChat package (version 1.5.0) based on the curated ligand–receptor interaction database known as CellChatDB(42). In brief, the data matrix of nasal polyp tissues was converted from the Seurat object to a CellChat object using the createCellChat function. The total numbers of interactions and interaction strengths were computed using the computeCommunProb function, and the communication probabilities for each cell signaling pathway were calculated using the

computeCommunProbPathway function.

IL-13 and IL-17 signature score analysis in chronic rhinosinusitis patients

The IL-13/IL-17 signature score was obtained using IL-13/IL-17 pathway-related genes as previously reported and validated(75). We integrated the scRNA-sequencing data of control mucosa from normal ethmoid or sphenoid sinuses (HRA000772) and polyp tissues from CRSwNP patients(57). The dataset consisted of 5 healthy controls, 7 neCRSwNP samples, and 10 eCRSwNP samples. The entire data processing pipeline, quality control, dimension reduction, clustering, and cell type annotation were assessed as described above (data not shown). Heatmaps were visualized with the ComplexHeatmap R package(76).

Tissue immunohistochemistry

Tissue immunohistochemical staining was performed as previously described(77). Immunohistochemical staining of neutrophil elastase with a monoclonal antibody (NE, 1:800, ab131260, Abcam) was applied to assess neutrophil infiltration. Sections were evaluated by 2 independent observers who were blinded to the groups and treatments.

Tissue immunofluorescence

Tissue immunohistochemical staining was also performed as previously described(22). To determine the localization of OSMR, immunofluorescence staining was conducted with OSMR (1:200, 10982-1-AP, Proteintech), DAPI for nuclei, VWF (Von Willebrand factor, 1:200, ab6994, Abcam) for endothelial cells, E-CAD (E-cadherin, 1:400, 3195s, CST) for epithelial cells, and COL1A1 (collagen, type I, alpha 1, 1:400, 72026s, CST) for fibroblasts.

Quantitative real-time reverse transcription PCR and cytokine measurement

Total RNA was extracted from tissue and cell samples using an RNA Easy Fast Tissue/Cell Kit (DP451, Tiangen Biotech, China) and then reverse transcribed to cDNA with a PrimeScript RT Master Mix Kit (RR036, TaKaRa, Japan). Quantitative real-time (RT) reverse transcription PCR was conducted using SYBR premix (RR820, Takara, Japan) with appropriate primers. Specific primers and TaqMan probes (Supplemental Table 4) were used to perform the quantitative RT–PCR amplification reactions.

The protein levels of ECP (7618E, MBL, USA), G-CSF (EK0360, Boster, China), IL-8 (EHC008.96, Neobioscience, China), periostin (EK0985, Boster, China), and CCL26 (DY347, R&D Systems, USA) in the cell culture supernatants were detected by using commercial ELISA kits according to the manufacturer's instructions. OSM, IFN-γ, IL-5, IL-13, GM-CSF, and IL-17A were analyzed using a custom Human Cytokine/Chemokine Panel II Kit (Millipore, USA).

Isolation and in vitro cell stimulation

As previously described(22), neutrophils were isolated from the PB samples of healthy volunteers via Ficoll hypaque gradient centrifugation and CD16 microbeads (130-045-701, Miltenyi, Germany). The purified neutrophils were stimulated with G-CSF (25 ng/mL, 300-23, Peprotech, China), GM-CSF (25 ng/mL, 300-03, Peprotech, China), and LPS (10 μg/mL, tlrl-eblps, Invitrogen, USA) in RPMI 1640 supplemented with 10% FBS for 4 h, after which the cells were harvested for further analysis.

Human nasal epithelial cells (HNECs) were cultured in BEGM, and fibroblasts were cultured in RPMI 1640 supplemented with 10% FBS(22). HNECs and fibroblasts were

stimulated with OSM (10 ng/mL, 8475-OM, R&D Systems, USA), IL-17A (10 ng/mL, 317-ILB-050, R&D Systems, USA), or IL-13 (10 ng/mL, 213-ILB-010, R&D Systems) for 12 h or 24 h. Cultured cells and their supernatants were collected for further analysis.

Flow cytometric analysis of peripheral blood and polyp tissue

PB samples were collected from patients before surgery. Nasal polyp tissues were collected within 30 min of the surgical procedure. The preparation of single-cell suspensions from both PB and nasal polyp samples followed the same procedure outlined earlier for scRNA-sequencing suspension preparation. Cell surface staining was performed for 30 min at 4 °C with the following human fluorochrome-conjugated antibodies: CD45, CD66B, CD16, CD62L, CXCR1 and CXCR2. The primary antibodies used are listed in Supplemental Table 5. The stained cells were analyzed immediately on a FACS Celesta cytometer (BD Biosciences) using FlowJo (version 10.0).

Statistical analysis

All data are presented as the means ± SDs and were analyzed using R (version 4.1.2), GraphPad Prism (version 8.0, GraphPad Software, Inc., San Diego, CA, USA), and SPSS (version 23.0, IBM Corporation, Armonk, NY, USA). Group differences were analyzed by one-way ANOVA, the Kruskal–Wallis or Dunn multiple comparison test or the Mann–Whitney test. Correlations were analyzed by Spearman's rank test. $P < 0.05$ was considered to indicate statistical significance with Bonferroni correction for multiple comparisons.

Study approval

All subjects signed the informed consent form, and the study was approved by the Ethics

Committee of the Eye & ENT Hospital of Fudan University.

Data availability

Raw sequencing data reported in this paper have been deposited at Genome Sequence Archive HRA006614. Other data that support the findings of this study were available from the corresponding authors upon reasonable request.

Authors' contributions

X.S., H.W., L.H., and D.W. conceived, supervised, and supported study; H.W., C.Z., and Q.Z. established the methodology of nasal tissue dissection, processing, and cell isolation; C.Z., Q.Z., and J.C. performed tissue dissection, immunostaining analysis, and in vitro studies; F.C., Y.W., Y.G., Yu.Z., and Y.Y. performed procurement of nasal tissue and analysis of immunostaining data; C.Z. performed the analysis of scRNA-sequencing data; H.L., L.S., K.X., H.Y., and D.W. provided nasal tissue samples for cell culture; X.S., H.W., L.H., and D.W. assisted with clinical expertise and resources; Ya.Z, H.W., and X.S. performed integrated data analysis and interpretation of data; C.Z., Q.Z., and H.W. wrote the manuscript. All authors read and approved the final version of the manuscript, take responsibility for its content, and agreed to submission.

Acknowledgments

We thank Dr. Jianming Zeng (University of Macau), and all the members of his bioinformatics team, biotrainee, for generously sharing their experience and codes. We sincerely appreciate the support provided by the Medical Science Data Center of Fudan University. We thank OE Biotech Co., Ltd. (Shanghai, China) for their contribution to the

scRNA-sequencing. This study was financially supported by the following programs and organizations: Natural Science Foundation of China (82000956); Natural Science Foundation of Tibet Autonomous Region (XZ2023ZR-ZY38(Z), XZ202401ZR0001)); Natural Science Foundation of Shigatse (RKZ2023ZR-001(Z) and RKZ2023ZR-008(Z)); Natural Science Foundation of Shanghai (21ZR1411700).

Declaration of Competing interests

The authors have no conflicts of interest to report.

References

1. Fokkens WJ, et al. European Position Paper on Rhinosinusitis and Nasal Polyps 2020. *Rhinology.* 2020;58(Suppl S29):1-464.
2. Orlandi RR, et al. International consensus statement on allergy and rhinology: rhinosinusitis 2021. *Int Forum Allergy Rhinol.* 2021;11(3):213-739.
3. Kato A, et al. Endotypes of chronic rhinosinusitis: Relationships to disease phenotypes, pathogenesis, clinical findings, and treatment approaches. *Allergy.* 2022;77(3):812-26.
4. Yao Y, et al. Revisiting Asian chronic rhinosinusitis in the era of type 2 biologics. *Clin Exp Allergy.* 2022;52(2):231-43.
5. Wang X, et al. Endotypes of chronic rhinosinusitis based on inflammatory and remodeling factors. *The Journal of allergy and clinical immunology.* 2023;151(2):458-68.
6. Poposki JA, et al. Elevation of activated neutrophils in chronic rhinosinusitis with nasal polyps. *J Allergy Clin Immunol.* 2022;149(5):1666-74.
7. Delemarre T, et al. A substantial neutrophilic inflammation as regular part of severe type 2 chronic rhinosinusitis with nasal polyps. *The Journal of allergy and clinical immunology.* 2021;147(1):179-88 e2.
8. Succar EF, et al. Neutrophils are underrecognized contributors to inflammatory burden and quality of life in chronic rhinosinusitis. *Allergy.* 2020;75(3):713-6.
9. Lim S, et al. Neutrophil extracellular traps promote DeltaNp63+ basal cell hyperplasia in chronic rhinosinusitis. *J Allergy Clin Immunol.* 2024;153(3):705-17 e11.
10. Shi LL, et al. Features of airway remodeling in different types of Chinese chronic rhinosinusitis are associated with inflammation patterns. *Allergy.* 2013;68(1):101-9.
11. Wu Y, et al. Neutrophil profiling illuminates anti-tumor antigen-presenting potency. *Cell.* 2024;187(6):1422-39 e24.
12. Kapellos TS, et al. Systemic alterations in neutrophils and their precursors in early-stage chronic obstructive pulmonary disease. *Cell Rep.* 2023;42(6):112525.
13. Xue R, et al. Liver tumour immune microenvironment subtypes and neutrophil heterogeneity. *Nature.* 2022;612(7938):141-7.

14. Wigerblad G, et al. Single-Cell Analysis Reveals the Range of Transcriptional States of Circulating Human Neutrophils. *J Immunol.* 2022.
15. Iwasaki N, et al. Analysis of Nasal Polyp Neutrophils by Single Cell RNA-Sequencing. *J Allergy Clin Immun.* 2023;151(2):Ab218-Ab.
16. Kamp VM, et al. Human suppressive neutrophils CD16bright/CD62Ldim exhibit decreased adhesion. *J Leukoc Biol.* 2012;92(5):1011-20.
17. Wang L, et al. Single-cell RNA-seq analysis reveals BHLHE40-driven pro-tumour neutrophils with hyperactivated glycolysis in pancreatic tumour microenvironment. *Gut.* 2022.
18. Xie X, et al. Single-cell transcriptome profiling reveals neutrophil heterogeneity in homeostasis and infection. *Nature Immunology.* 2020;21(9):1119-33.
19. Chasset F, et al. Identification of highly active systemic lupus erythematosus by combined type I interferon and neutrophil gene scores vs classical serologic markers. *Rheumatology (Oxford).* 2020;59(11):3468-78.
20. Pothoven KL, et al. Oncostatin M promotes mucosal epithelial barrier dysfunction, and its expression is increased in patients with eosinophilic mucosal disease. *J Allergy Clin Immun.* 2015;136(3):737-46.e4.
21. Headland SE, et al. Oncostatin M expression induced by bacterial triggers drives airway inflammatory and mucus secretion in severe asthma. *Sci Transl Med.* 2022;14(627):eabf8188.
22. Zhang C, et al. Lipocalin-2 promotes neutrophilic inflammation in nasal polyps and its value as biomarker. *Allergol Int.* 2023.
23. Bertelsen T, et al. IkappaBzeta is a key player in the antipsoriatic effects of secukinumab. *The Journal of allergy and clinical immunology.* 2020;145(1):379-90.
24. Wang H, et al. The activation and function of IL-36gamma in neutrophilic inflammation in chronic rhinosinusitis. *J Allergy Clin Immunol.* 2018;141(5):1646-58.
25. Arebro J, et al. Subsetting reveals CD16(high) CD62L(dim) neutrophils in chronic rhinosinusitis with nasal polyps. *Allergy.* 2019;74(12):2499-501.
26. Wei Y, et al. Activated pyrin domain containing 3 (NLRP3) inflammasome in neutrophilic chronic rhinosinusitis with nasal polyps (CRSwNP). *J Allergy Clin Immunol.* 2020.
27. Zhong B, et al. HIF-1alpha activates NLRP3 inflammasome to regulate epithelial differentiation in chronic rhinosinusitis. *J Allergy Clin Immunol.* 2023.
28. Zhong B, et al. HIF-1α induces NLRP3 expression by M1 macrophages in non-eosinophilic chronic rhinosinusitis with nasal polyps. *Allergy.* 2020.
29. Zhang D, et al. Neutrophil ageing is regulated by the microbiome. *Nature.* 2015;525(7570):528-32.
30. Aroca-Crevillen A, et al. Neutrophils in Physiology and Pathology. *Annu Rev Pathol.* 2024;19:227-59.
31. Gupta S, et al. Sex differences in neutrophil biology modulate response to type I interferons and immunometabolism. *Proc Natl Acad Sci U S A.* 2020;117(28):16481-91.
32. Glennon-Alty L, et al. Type I interferon regulates cytokine-delayed neutrophil apoptosis, reactive oxygen species production and chemokine expression. *Clin Exp Immunol.* 2021;203(2):151-9.
33. Ji L, et al. The crucial regulatory role of type I interferon in inflammatory diseases. *Cell Biosci.* 2023;13(1):230.
34. Wen W, et al. Increased neutrophilia in nasal polyps reduces the response to oral corticosteroid therapy. *J Allergy Clin Immunol.* 2012;129(6):1522-8 e5.

35. Hu XT, et al. Enhanced oxidative stress is associated with tissue neutrophilia and poor steroid response in chronic rhinosinusitis with nasal polyps. *World J Otorhinolaryngol Head Neck Surg.* 2023;9(4):320-7.
36. Tsai CH, et al. Neutrophil extracellular trap production and CCL4L2 expression influence corticosteroid response in asthma. *Sci Transl Med.* 2023;15(699):eadf3843.
37. Impellizzieri D, et al. IL-4 receptor engagement in human neutrophils impairs their migration and extracellular trap formation. *J Allergy Clin Immunol.* 2019;144(1):267-79.e4.
38. Gevaert E, et al. Charcot-Leyden crystals promote neutrophilic inflammation in patients with nasal polyposis. *J Allergy Clin Immunol.* 2020;145(1):427-30 e4.
39. Chen J, et al. Comparative short-term efficacy of endoscopic sinus surgery and biological therapies in chronic rhinosinusitis with nasal polyps: A network meta-analysis. *Clin Transl Allergy.* 2023;13(6):e12269.
40. Kotas ME, et al. IL-13-associated epithelial remodeling correlates with clinical severity in nasal polyposis. *J Allergy Clin Immunol.* 2023.
41. Chen CC, et al. IL-4Ralpha signaling promotes barrier-altering oncostatin M and IL-6 production in aspirin-exacerbated respiratory disease. *J Allergy Clin Immunol.* 2024.
42. Jin S, et al. Inference and analysis of cell-cell communication using CellChat. *Nat Commun.* 2021;12(1):1088.
43. Pothoven KL, et al. Neutrophils are a major source of the epithelial barrier disrupting cytokine oncostatin M in patients with mucosal airways disease. *J Allergy Clin Immunol.* 2017;139(6):1966-78.e9.
44. Wang B-F, et al. Evidence that oncostatin M synergizes with IL-4 signaling to induce TSLP expression in chronic rhinosinusitis with nasal polyps. *Journal of Allergy and Clinical Immunology.* 2023.
45. Li Z, et al. 15-Lipoxygenase 1 in nasal polyps promotes CCL26/eotaxin 3 expression through extracellular signal-regulated kinase activation. *The Journal of allergy and clinical immunology.* 2019.
46. Wang M, et al. Association of periostin expression with eosinophilic inflammation in nasal polyps. *The Journal of allergy and clinical immunology.* 2015;136(6):1700-3 e9.
47. Min JY, et al. Proton pump inhibitors decrease eotaxin-3/CCL26 expression in patients with chronic rhinosinusitis with nasal polyps: Possible role of the nongastric H,K-ATPase. *The Journal of allergy and clinical immunology.* 2017;139(1):130-41 e11.
48. Ryu G, et al. Role of IL-17A in Chronic Rhinosinusitis With Nasal Polyp. *Allergy, asthma & immunology research.* 2020;12(3):507-22.
49. Klingler AI, et al. Mechanisms and biomarkers of inflammatory endotypes in chronic rhinosinusitis without nasal polyps. *The Journal of allergy and clinical immunology.* 2021;147(4):1306-17.
50. Kwofie K, et al. Regulation of IL-17A responses in human airway smooth muscle cells by Oncostatin M. *Respir Res.* 2015;16(1):14.
51. Nagahama KY, et al. Oncostatin M modulates fibroblast function via signal transducers and activators of transcription proteins-3. *Am J Respir Cell Mol Biol.* 2013;49(4):582-91.
52. Slowikowski K, et al. CUX1 and IkappaBzeta (NFKBIZ) mediate the synergistic inflammatory response to TNF and IL-17A in stromal fibroblasts. *Proc Natl Acad Sci U S A.* 2020;117(10):5532-41.
53. Muller A, et al. IkappaBzeta is a key transcriptional regulator of IL-36-driven psoriasis-related gene expression in keratinocytes. *Proc Natl Acad Sci U S A.* 2018;115(40):10088-93.

54. Taylor TC, et al. IkappaBzeta is an essential mediator of immunity to oropharyngeal candidiasis. *Cell Host Microbe.* 2023;31(10):1700-13 e4.
55. Muromoto R, et al. Regulation of NFKBIZ gene promoter activity by STAT3, C/EBPbeta, and STAT1. *Biochem Biophys Res Commun.* 2022;613:61-6.
56. Mortuaire G, et al. Lund-Mackay score is predictive of bleeding in ethmoidectomy for nasal polyposis. *Rhinology.* 2008;46(4):285-8.
57. Wang W, et al. Single-cell profiling identifies mechanisms of inflammatory heterogeneity in chronic rhinosinusitis. *Nat Immunol.* 2022;23(10):1484-94.
58. Sinha S, et al. Dexamethasone modulates immature neutrophils and interferon programming in severe COVID-19. *Nat Med.* 2022;28(1):201-11.
59. 10xGenomics. Capturing Neutrophils in 10x Single Cell Gene Expression Data. https://support.10xgenomics.com/single-cell-gene-expression/software/pipelines/latest/tutorials/neutrophils.
60. Butler A, et al. Integrating single-cell transcriptomic data across different conditions, technologies, and species. *Nat Biotechnol.* 2018;36(5):411-20.
61. Hao Y, et al. Integrated analysis of multimodal single-cell data. *Cell.* 2021;184(13):3573-87 e29.
62. Hafemeister C, and Satija R. Normalization and variance stabilization of single-cell RNA-seq data using regularized negative binomial regression. *Genome Biol.* 2019;20(1):296.
63. Korsunsky I, et al. Fast, sensitive and accurate integration of single-cell data with Harmony. *Nat Methods.* 2019;16(12):1289-96.
64. Zappia L, and Oshlack A. Clustering trees: a visualization for evaluating clusterings at multiple resolutions. *Gigascience.* 2018;7(7).
65. Ordovas-Montanes J, et al. Allergic inflammatory memory in human respiratory epithelial progenitor cells. *Nature.* 2018;560(7720):649-54.
66. Mabbott NA, et al. An expression atlas of human primary cells: inference of gene function from coexpression networks. *BMC Genomics.* 2013;14:632.
67. Zhang L, et al. Lineage tracking reveals dynamic relationships of T cells in colorectal cancer. *Nature.* 2018;564(7735):268-72.
68. Trapnell C, et al. The dynamics and regulators of cell fate decisions are revealed by pseudotemporal ordering of single cells. *Nat Biotechnol.* 2014;32(4):381-6.
69. Szklarczyk D, et al. The STRING database in 2023: protein-protein association networks and functional enrichment analyses for any sequenced genome of interest. *Nucleic Acids Res.* 2023;51(D1):D638-D46.
70. Cline MS, et al. Integration of biological networks and gene expression data using Cytoscape. *Nat Protoc.* 2007;2(10):2366-82.
71. Wu T, et al. clusterProfiler 4.0: A universal enrichment tool for interpreting omics data. *Innovation (Camb).* 2021;2(3):100141.
72. Saul D, et al. A new gene set identifies senescent cells and predicts senescence-associated pathways across tissues. *Nat Commun.* 2022;13(1):4827.
73. Alvarez MJ, et al. Functional characterization of somatic mutations in cancer using network-based inference of protein activity. *Nat Genet.* 2016;48(8):838-47.
74. Holland CH, et al. Robustness and applicability of transcription factor and pathway analysis tools on single-cell RNA-seq data. *Genome Biol.* 2020;21(1):36.
75. Christenson SA, et al. An airway epithelial IL-17A response signature identifies a steroid-unresponsive COPD patient subgroup. *J Clin Invest.* 2019;129(1):169-81.
76. Gu Z, et al. Complex heatmaps reveal patterns and correlations in multidimensional genomic data. *Bioinformatics.* 2016;32(18):2847-9.

77. Zhang C, et al. Subjective symptoms as predictors for eosinophilic chronic rhinosinusitis with nasal polyps in the Chinese population. *Eur Arch Otorhinolaryngol.* 2023;280(8):3721-9.

Figure legends

Figure 1. ScRNA-sequencing profiling maps the heterogeneity of neutrophils in nasal polyps. (A) Graphical scheme describing the experimental workflow. (B) UMAP plot depicting the major cell types identified by single-cell sequencing; bar plot depicting the proportion of cell subsets. (C) UMAP plot displaying the marker gene expression of neutrophils. (D) UMAP plot depicting the neutrophils by groups. (E) Trajectory of neutrophils along pseudotime in a two-dimensional space. Each point corresponds to a single cell. (F) Heatmap showing the dynamic gene expression changes over pseudotime. The differentially expressed genes were clustered hierarchically into three groups. (J) Volcano plots showing changes in the neCRSwNP neutrophils compared to the PB neutrophils. (H) the core network calculated by MCODE in the protein–protein interaction (PPI) network for upregulated genes in the neCRSwNP neutrophils compared to the PB neutrophils. Score = 13.000. (I) Volcano plots exhibiting changes in eCRSwNP neutrophils compared to PB neutrophils. (J) the core network calculated by MCODE in the PPI network for upregulated genes in eCRSwNP neutrophils compared to PB neutrophils. Score = 8.909.

Figure 2. Neutrophils are activated in both eCRSwNPs and neCRSwNPs. (A) Violin plot showing the signature score of the neutrophil activation (GO:0042119) pathway and the expression levels of pathway-related genes in each group of neutrophils. (B) Violin plot showing the signature score of the inflammasome pathway in each group of neutrophils; (C) Dot plot depicting the expression levels of inflammasome components in each group of neutrophils. (D) Representative images of neutrophil elastase (NE) immunohistochemical staining under high magnification were selected, and the number of NE-positive cells was quantified in high-power fields (HPF) with the Kruskal-Wallis test

with Dunn's post hoc test. (control: n = 7, neCRSwNP: n = 20, eCRSwNP: n = 55). (E) Scatter plot depicting the NE expression level of tissue homogenates in the control uncinate tissues (UTs) (n = 17), neCRSwNP (n = 27), and eCRSwNP (n = 34) groups with the Kruskal-Wallis test with Dunn's post hoc test. (F) Representative flow cytometry plots showing the activated neutrophils (CD62L-) within the live CD45+CD66B+CD16+ population. (G) Representative histograms of flow cytometry showing the levels of CD62L by geometric mean fluorescence intensity (gMFI). (H) Box-and-whisker plots presenting the differences in the CD62L gMFI ratio on neutrophils with the Kruskal-Wallis test with Dunn's post hoc test (PB: n = 19, neCRSwNP: n = 10, eCRSwNP: n = 11). (I) Box-and-whisker plot presenting the frequency of CD62-negative neutrophils with the Kruskal-Wallis test with Dunn's post hoc test (PB: n = 19, neCRSwNP: n = 10, eCRSwNP: n = 11). * $p<0.05$, ** $p<0.01$, *** $p<0.001$, **** $p<0.001$.

Figure 3. Neutrophils in nasal polyps consist of distinct transcriptional subsets. (A) The UMAP plot depicting 10 clusters of neutrophils; (B) Line graphs presenting the ratio of observed to expected cell numbers (Ro/e) for each cluster. (C) Dot plot depicting the top 3 genes in each neutrophil cluster. (D) UMAP plot depicting 5 subsets of neutrophils. (E) Heatmap showing the Ro/e level of each subset. (F) Box-and-whisker plot depicting the proportions of neutrophil subsets in different groups. (G) Heatmap visualizing the 40 genes with the highest expression levels and pathway enrichment for each neutrophil subset. (H) The violin plot showing the signature score of the senescence pathway in different neutrophil subsets. (I) The violin plot showing the signature score of the neutrophil activation pathway in different neutrophil subsets. (J) The density heatmap displaying the signature score of the response to type I interferon pathway in neutrophils. The violin plot

showing the signature score of the response to type I interferon pathway in the neCRSwNPs. (K) The dot plot depicting the gene expression level related to the response to type I interferon pathway in different neutrophil subsets. (L) The scatter plot showing the correlation between the signature score of the response to type I interferon pathway and the average MX1 expression level in the scRNA-sequencing data of nasal polyps with Spearman's rank test. (M) The scatter dot plot displaying the MX1 mRNA level in control UTs and nasal polyps with the Kruskal-Wallis test with Dunn's post hoc test (control: n = 13, neCRSwNP: n = 14, eCRSwNP: n = 14). * $p<0.05$, ** $p<0.01$, *** $p<0.001$, **** $p<0.001$.

Figure 4. The transcriptional modulation of different neutrophil subsets in eCRSwNPs and neCRSwNPs. (A) Heatmap showing the top 5 gene expression levels for each group in different neutrophil subsets. (B) Violin plot showing the expression levels of C-X-C chemokine receptor type 1 (CXCR1), and CXCR2 in each neutrophil subset. (C) Representative flow cytometry histograms showing the levels of CXCR1. Box-and-whisker plots showing the differences in the CXCR1 MFI ratio in NP neutrophils with the Mann-Whitney U test (neCRSwNP: n = 5; eCRSwNP: n = 6). (D) Representative flow cytometry histograms showing the levels of CXCR2 and box-and-whisker plots showing the differences in the CXCR2 MFI ratio in NP neutrophils with the Mann-Whitney U test (neCRSwNP: n = 5; eCRSwNP: n = 6). * $p<0.05$, ** $p<0.01$, *** $p<0.001$, **** $p<0.001$.

Figure 5. The level of OSM secreted by neutrophils is elevated in CRSwNP. (A) Heatmap showing the outgoing signaling patterns when neutrophils were selected as sender cells via the CellChat algorithm. (B) Heatmap showing the incoming signaling patterns when neutrophils were selected as sender cells via the CellChat algorithm. (C) Chord diagrams

of the signaling pathway network displaying secreting and receiving cells of OSM signaling. (D) UMAP plot depicting the distribution of OSM in the scRNA-sequencing data. (E) Violin plot depicting the OSM expression level; UMAP plot depicting the distribution of OSM in neutrophils of the scRNA-sequencing data. (F) Scatter dot plot depicting the protein levels of OSM in control UT (n = 17), neCRSwNP (n = 27), and eCRSwNP (n = 34) groups in tissue homogenates with the Kruskal-Wallis test with Dunn's post hoc test. (G) Violin plot showing the expression levels of the OSM receptors, including gp130 (IL6ST), LIFRα (LIFT), and OSMRβ (OSMR). (H) Representative images of OSMR, VWF (a biomarker of endothelial cells), E-CAD (a biomarker of epithelial cells), and COL1A1 (a biomarker of fibroblasts) immunofluorescence staining in NPs. (I) Scatter dot plot displaying the OSMR mRNA level in control UTs and nasal polyps with the Kruskal-Wallis test with Dunn's post hoc test (control: n = 9; neCRSwNP: n = 17; eCRSwNP: n = 19). (J) Heatmap of correlation presenting the correlation between the signature score of the response to LPS pathway and the expression level of common up-regulated cytokines/chemokines in neCRSwNP and eCRSwNP neutrophils with Spearman's rank test. (K) The GSEA plots showing the enrichment of response to lipopolysaccharide in the eCRSwNP or neCRSwNP neutrophils compared to the PB neutrophils. (L) The scatter dot plot depicting the protein levels of G-CSF and GM-CSF in control UT (n = 17), neCRSwNP (n = 27), and eCRSwNP (n = 34) tissue homogenates with the Kruskal-Wallis test with Dunn's post hoc test. (M) The scatter plot visualizing the correlation of OSM and GM-CSF expression level in tissue homogenates of nasal polyps with Spearman's rank test. (N) The histogram displaying OSM mRNA level in neutrophils after stimulation of LPS, G-CSF, and GM-CSF with the Kruskal-Wallis test with Dunn's

post hoc test (n = 4). * $p<0.05$, ** $p<0.01$, *** $p<0.001$, **** $p<0.001$.

Figure 6. OSM modulates pathogenic pathways in epithelial cells and fibroblasts depending on inflammatory patterns. (A) The scatter plot showing the correlation of ECP and elastase with OSM expression in eCRSwNP tissue homogenates. (B) The violin plot showing the signature score of the IL-13 pathway in fibroblasts and epithelial cells of the nasal mucosa. (C) The scatter dot plot depicting the protein levels of CCL26 and periostin in control UT (n = 17), neCRSwNP (n = 27), and eCRSwNP (n = 34) tissue homogenates with the Kruskal-Wallis test with Dunn's post hoc test. (D) The heatmap showing the expression levels of CCL26 and periostin in the scRNA-sequencing data. (E) The histogram displaying CCL26 and periostin secretion in culture supernatants after 24 h of stimulation in fibroblasts. (F) The histogram displaying CCL26 and periostin secretion in culture supernatants after 24 h of stimulation with the Kruskal-Wallis test with Dunn's post hoc test (n = 6). (G) The histogram displaying IL-13 receptor mRNA levels (IL4R, IL2RG, IL13RA1, and IL13RA2) in fibroblasts after 12 h of stimulation with OSM with the Mann-Whitney U test (n = 4). Scatter plot displaying the correlation between the IL4R expression level in fibroblasts and the total OSM expression level in the scRNA-sequencing data of polyp samples with Spearman's rank test. (H) Scatter plot showing the correlation between elastase, IL-17A, G-CSF, IL-6, and IL-8 and the OSM expression level in neCRSwNP tissue homogenates with Spearman's rank test. (I) Heatmap showing the IL-17 pathway score in fibroblasts and epithelial cells of healthy controls with normal ethmoid or sphenoid sinuses and nasal polyps in the scRNA-sequencing data. (J) Heatmap showing the expression levels of G-CSF and IL-8 in the scRNA-sequencing data. (K) Histogram displaying the G-CSF and IL-8 secretion in culture supernatants after 12 h of stimulation

899 in fibroblasts with the Kruskal-Wallis test with Dunn's post hoc test (n = 6). (L) Histogram
900 displaying the G-CSF and IL-8 secretion in culture supernatants after 12 h of stimulation
901 in HNECs with the Kruskal-Wallis test with Dunn's post hoc test (n = 6). * $p<0.05$, **
902 $p<0.01$, *** $p<0.001$, **** $p<0.001$.

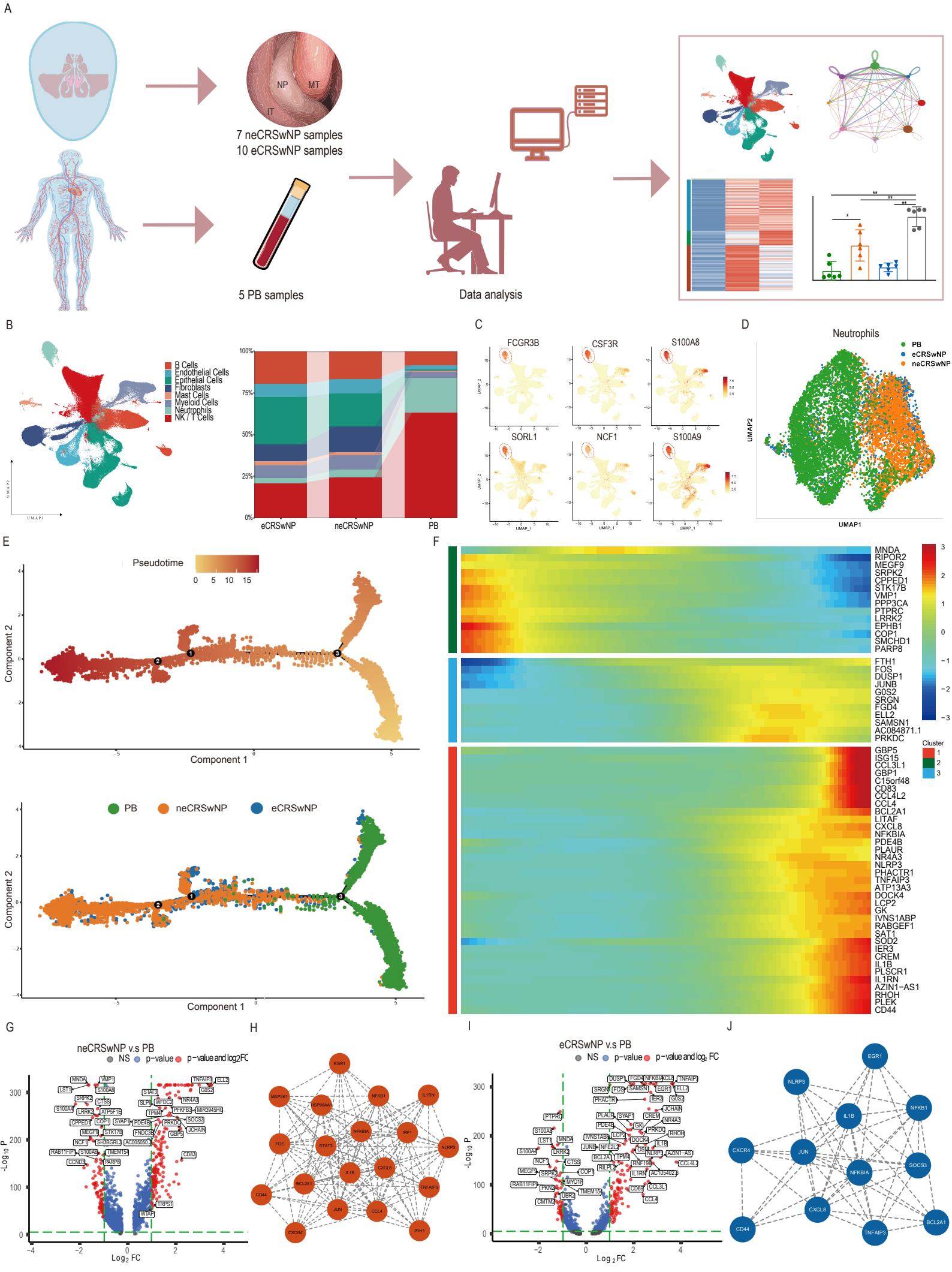
A
NP
MT
IT
7 neCRSwNP samples
10 eCRSwNP samples
5 PB samples
Data analysis
B
B Cells
Endothelial Cells
Epithelial Cells
Fibroblasts
Mast Cells
Myeloid Cells
Neutrophils
NK / T Cells
eCRSwNP
neCRSwNP
PB
C
FCGR3B
CSF3R
S100A8
SORL1
NCF1
S100A9
D
Neutrophils
PB
eCRSwNP
neCRSwNP
UMAP1
UMAP2
E
Pseudotime
Component 1
Component 2
PB
neCRSwNP
eCRSwNP
F
MNDA
RIPOR2
MEGF9
SRPK2
CPPED1
STK17B
VMP1
PPP3CA
PTPRC
LRRK2
EPHB1
COP1
SMCHD1
PARP8
FTH1
FOS
DUSP1
JUNB
G0S2
SRGN
FGD4
ELL2
SAMSN1
AC084871.1
PRKDC
GBP5
ISG15
CCL3L1
GBP1
C15orf48
CD83
CCL4L2
CCL4
BCL2A1
LITAF
CXCL8
NFKBIA
PDE4B
PLAUR
NR4A3
NLRP3
PHACTR1
TNFAIP3
ATP13A3
DOCK4
LCP2
GK
IVNS1ABP
RABGEF1
SAT1
SOD2
IER3
CREM
IL1B
PLSCR1
IL1RN
AZIN1-AS1
RHOH
PLEK
CD44
Cluster
1
2
3
G
neCRSwNP v.s PB
NS
p-value
p-value and log2FC
-Log10 P
Log2 FC
H
EGR1
MAP2K1
NFKB1
IL1RN
HSP90AA1
NFKBIA
IRF1
NLRP3
FOS
STAT3
IL1B
CXCL8
BCL2A
TNFAIP3
CD44
JUN
CCL4
CXCR4
IFIH1
I
eCRSwNP v.s PB
NS
p-value
p-value and log2 FC
-Log10 P
Log2 FC
J
EGR1
NLRP3
IL1B
NFKB1
CXCR4
JUN
SOCS3
NFKBIA
CXCL8
BCL2A1
CD44
TNFAIP3

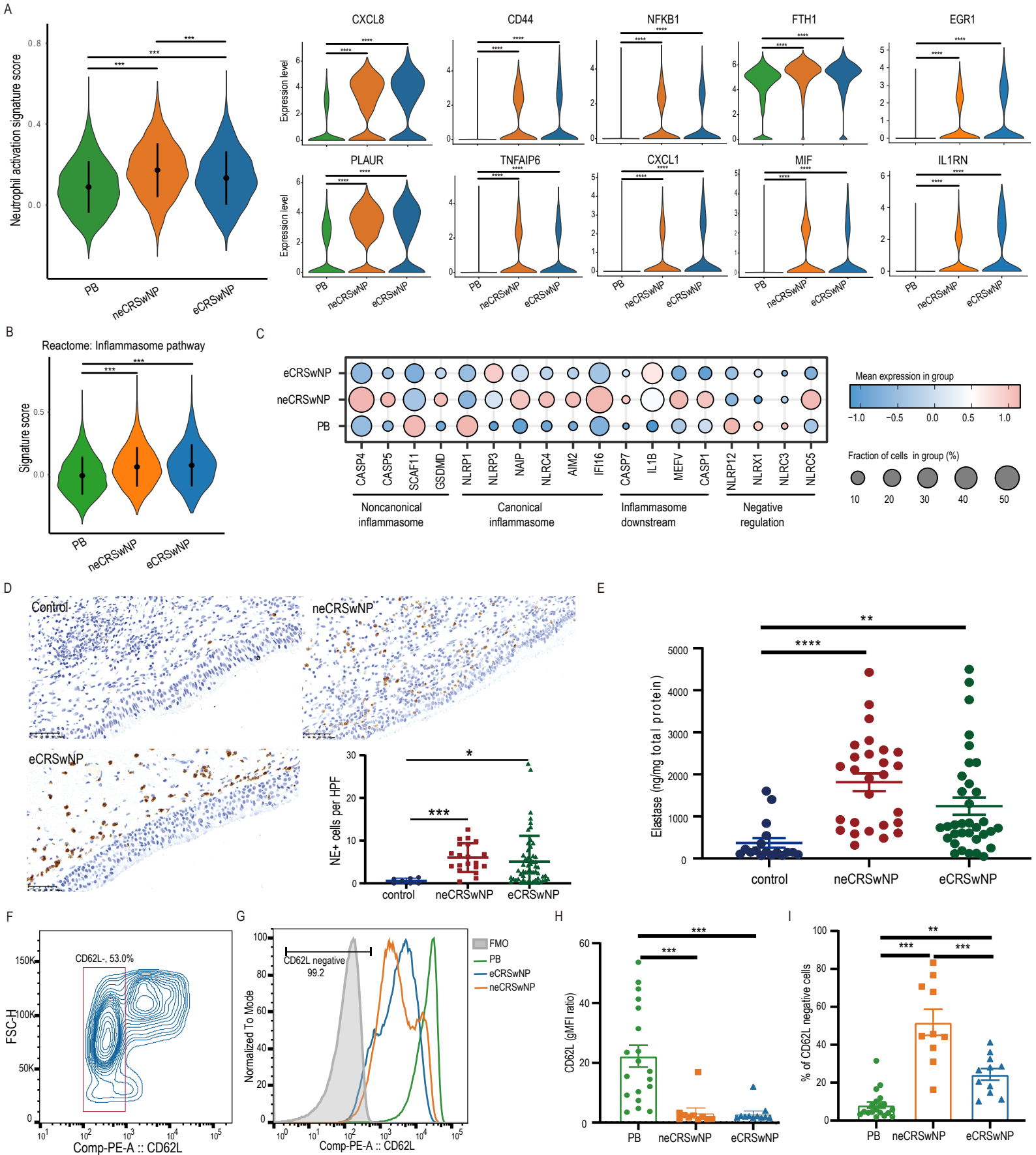
A
Neutrophil activation signature score
PB
neCRSwNP
eCRSwNP
CXCL8
CD44
NFKB1
FTH1
EGR1
PLAUR
TNFAIP6
CXCL1
MIF
IL1RN
Expression level
B
Reactome: Inflammasome pathway
Signature score
C
eCRSwNP
neCRSwNP
PB
CASP4
CASP5
SCAF11
GSDMD
NLRP1
NLRP3
NAIP
NLRC4
AIM2
IFI16
CASP7
IL1B
MEFV
CASP1
NLRP12
NLRX1
NLRC3
NLRC5
Noncanonical inflammasome
Canonical inflammasome
Inflammasome downstream
Negative regulation
Mean expression in group
Fraction of cells in group (%)
D
Control
neCRSwNP
eCRSwNP
NE+ cells per HPF
control
E
Elastase (ng/mg total protein)
F
CD62L-, 53.0%
FSC-H
Comp-PE-A :: CD62L
G
CD62L negative
99.2
Normalized To Mode
FMO
PB
eCRSwNP
neCRSwNP
H
CD62L (gMFI ratio)
I
% of CD62L negative cells

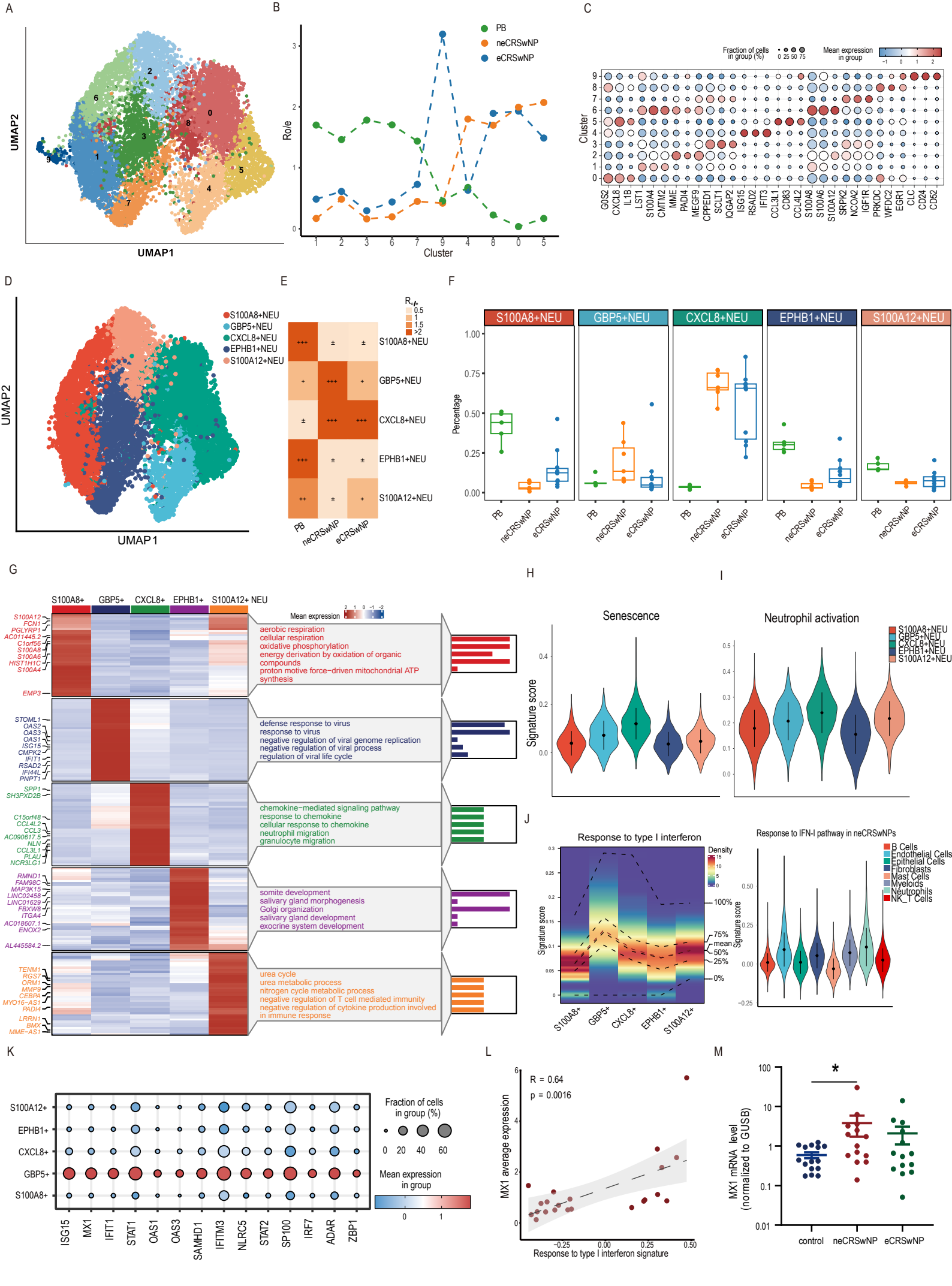
A
UMAP2
UMAP1
B
PB
neCRSwNP
eCRSwNP
Ro/e
Cluster
C
Fraction of cells in group (%)
Mean expression in group
Cluster
GOS2
CXCL8
IL1B
LST1
S100A4
CMTM2
MME
PADI4
MEGF9
CPPED1
SCLT1
IQGAP2
ISG15
RSAD2
IFIT3
CCL3L1
CD83
CCL4L2
S100A8
S100A6
S100A12
SRPK2
NCOA2
IGF1R
PRKDC
WFDC2
EGR1
CLC
CD24
CD52
D
S100A8+NEU
GBP5+NEU
CXCL8+NEU
EPHB1+NEU
S100A12+NEU
UMAP2
UMAP1
E
PB
neCRSwNP
eCRSwNP
F
Percentage
G
S100A8+
GBP5+
CXCL8+
EPHB1+
S100A12+ NEU
Mean expression
aerobic respiration
cellular respiration
oxidative phosphorylation
energy derivation by oxidation of organic compounds
proton motive force−driven mitochondrial ATP synthesis
defense response to virus
response to virus
negative regulation of viral genome replication
negative regulation of viral process
regulation of viral life cycle
chemokine−mediated signaling pathway
response to chemokine
cellular response to chemokine
neutrophil migration
granulocyte migration
somite development
salivary gland morphogenesis
Golgi organization
salivary gland development
exocrine system development
urea cycle
urea metabolic process
nitrogen cycle metabolic process
negative regulation of T cell mediated immunity
negative regulation of cytokine production involved in immune response
H
Senescence
Signature score
I
Neutrophil activation
J
Response to type I interferon
Density
Signature score
Response to IFN-I pathway in neCRSwNPs
B Cells
Endothelial Cells
Epithelial Cells
Fibroblasts
Mast Cells
Myeloids
Neutrophils
NK_T Cells
K
Fraction of cells in group (%)
Mean expression in group
ISG15
MX1
IFIT1
STAT1
OAS1
OAS3
SAMHD1
IFITM3
NLRC5
STAT2
SP100
IRF7
ADAR
ZBP1
L
R = 0.64
p = 0.0016
MX1 average expression
Response to type I interferon signature
M
MX1 mRNA level (normalized to GUSB)
control
neCRSwNP
eCRSwNP

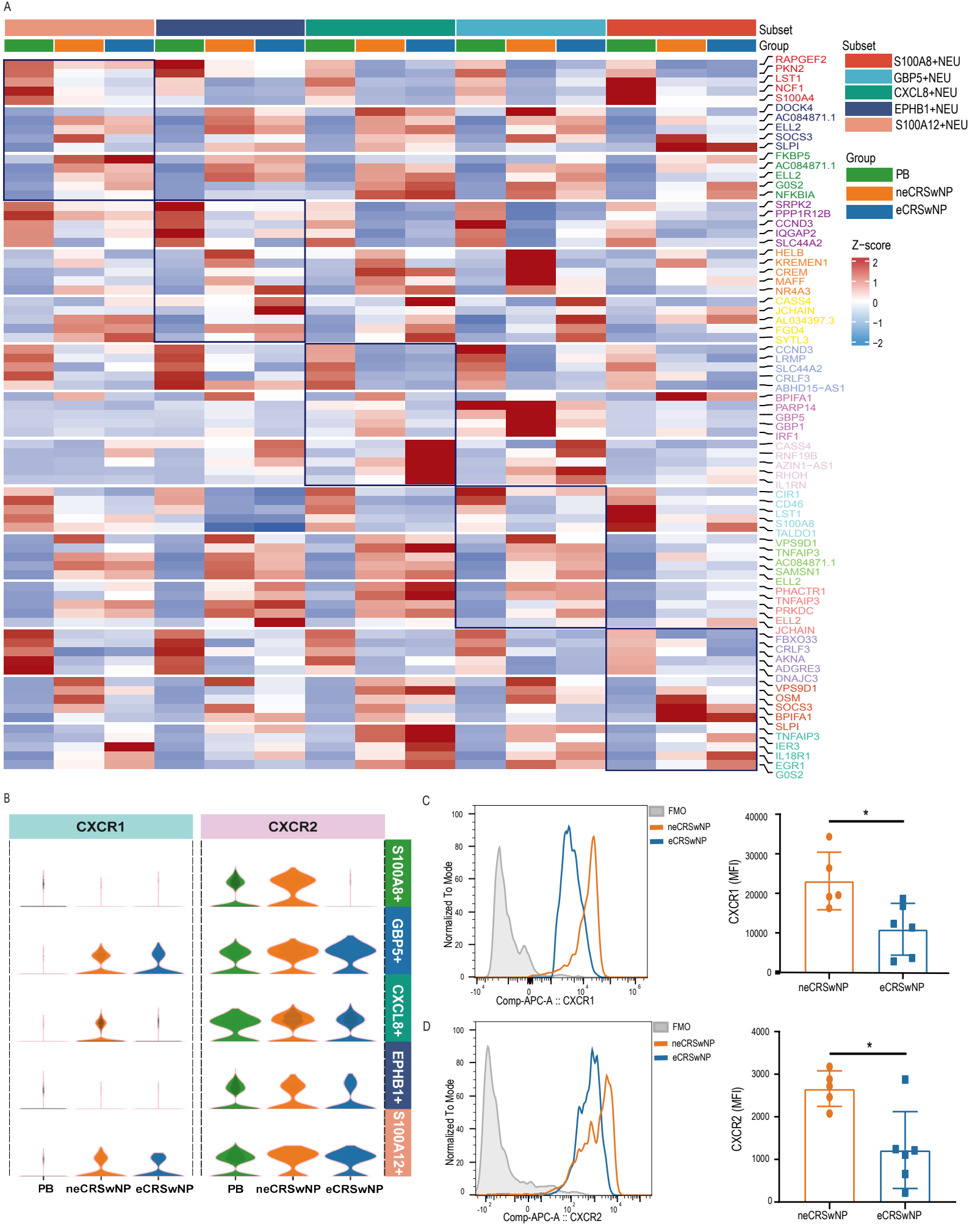
A
Subset
Group
Subset
S100A8+NEU
GBP5+NEU
CXCL8+NEU
EPHB1+NEU
S100A12+NEU
Group
PB
neCRSwNP
eCRSwNP
Z-score
2
1
0
−1
−2
RAPGEF2
PKN2
LST1
NCF1
S100A4
DOCK4
AC084871.1
ELL2
SOCS3
SLPI
FKBP5
AC084871.1
ELL2
G0S2
NFKBIA
SRPK2
PPP1R12B
CCND3
IQGAP2
SLC44A2
HELB
KREMEN1
CREM
MAFF
NR4A3
CASS4
JCHAIN
AL034397.3
FGD4
SYTL3
CCND3
LRMP
SLC44A2
CRLF3
ABHD15−AS1
BPIFA1
PARP14
GBP5
GBP1
IRF1
CASS4
RNF19B
AZIN1−AS1
RHOH
IL1RN
CIR1
CD46
LST1
S100A8
TALDO1
VPS9D1
TNFAIP3
AC084871.1
SAMSN1
ELL2
PHACTR1
TNFAIP3
PRKDC
ELL2
JCHAIN
FBXO33
CRLF3
AKNA
ADGRE3
DNAJC3
VPS9D1
OSM
SOCS3
BPIFA1
SLPI
TNFAIP3
IER3
IL18R1
EGR1
G0S2
B
CXCR1
CXCR2
S100A8+
GBP5+
CXCL8+
EPHB1+
S100A12+
PB
neCRSwNP
eCRSwNP
PB
neCRSwNP
eCRSwNP
C
FMO
neCRSwNP
eCRSwNP
Normalized To Mode
Comp-APC-A :: CXCR1
CXCR1 (MFI)
*
neCRSwNP
eCRSwNP
D
FMO
neCRSwNP
eCRSwNP
Normalized To Mode
Comp-APC-A :: CXCR2
CXCR2 (MFI)
*
neCRSwNP
eCRSwNP

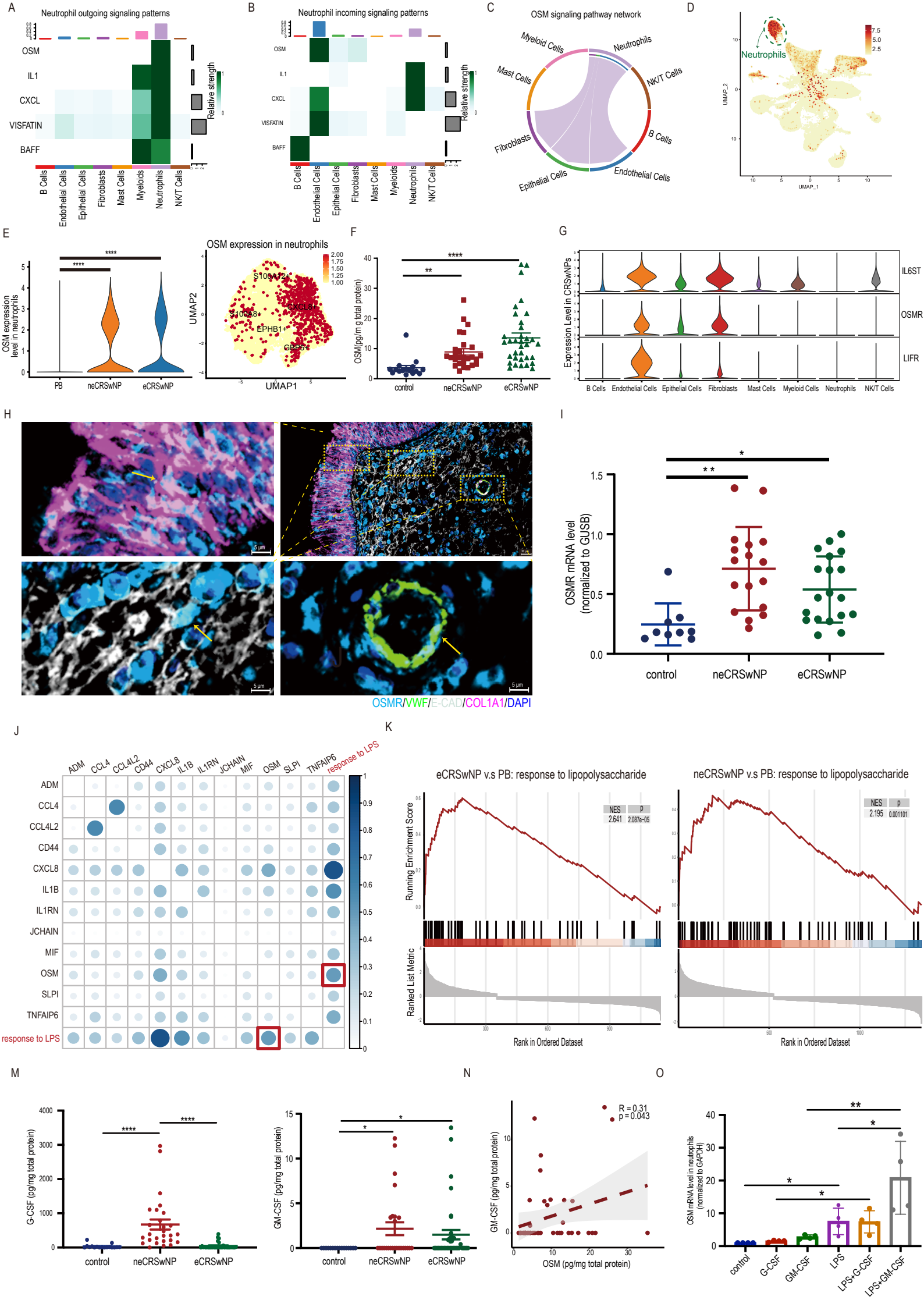
A
Neutrophil outgoing signaling patterns
OSM
IL1
CXCL
VISFATIN
BAFF
Relative strength
B Cells
Endothelial Cells
Epithelial Cells
Fibroblasts
Mast Cells
Myeloids
Neutrophils
NK/T Cells
B
Neutrophil incoming signaling patterns
C
OSM signaling pathway network
Myeloid Cells
Neutrophils
Mast Cells
NK/T Cells
B Cells
Fibroblasts
Endothelial Cells
Epithelial Cells
D
Neutrophils
UMAP_1
UMAP_2
E
OSM expression level in neutrophils
PB
neCRSwNP
eCRSwNP
OSM expression in neutrophils
S100A12+
S100A8+
CXCL8+
EPHB1+
GPR84+
UMAP1
UMAP2
F
OSM(pg/m g total protein)
control
neCRSwNP
eCRSwNP
G
Expression Level in CRSwNPs
IL6ST
OSMR
LIFR
B Cells
Endothelial Cells
Epithelial Cells
Fibroblasts
Mast Cells
Myeloid Cells
Neutrophils
NK/T Cells
H
OSMR/VWF/E-CAD/COL1A1/DAPI
I
OSMR mRNA level (normalized to GUSB)
control
neCRSwNP
eCRSwNP
J
ADM
CCL4
CCL4L2
CD44
CXCL8
IL1B
IL1RN
JCHAIN
MIF
OSM
SLPI
TNFAIP6
response to LPS
K
eCRSwNP v.s PB: response to lipopolysaccharide
neCRSwNP v.s PB: response to lipopolysaccharide
Running Enrichment Score
Ranked List Metric
Rank in Ordered Dataset
NES
p
2.641
2.087e-05
2.195
0.001101
M
G-CSF (pg/mg total protein)
GM-CSF (pg/mg total protein)
control
neCRSwNP
eCRSwNP
N
R = 0.31
p = 0.043
GM-CSF (pg/mg total protein)
OSM (pg/mg total protein)
O
OSM mRNA level in neutrophils (normalized to GAPDH)
control
G-CSF
GM-CSF
LPS
LPS+G-CSF
LPS+GM-CSF

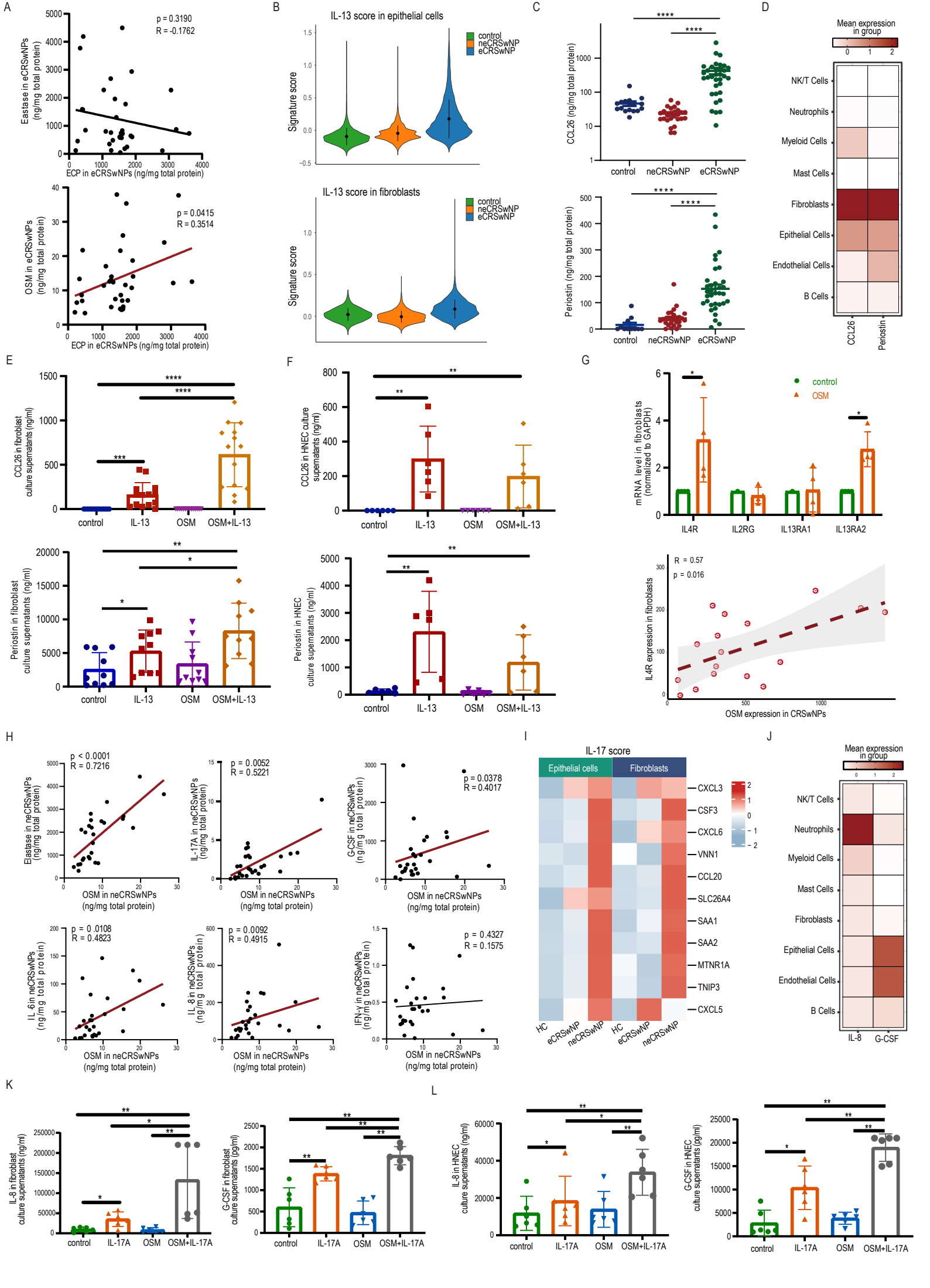
A
p = 0.3190
R = -0.1762
Eastase in eCRSwNPs (ng/mg total protein)
ECP in eCRSwNPs (ng/mg total protein)
p = 0.0415
R = 0.3514
OSM in eCRSwNPs (ng/mg total protein)
B
IL-13 score in epithelial cells
control
neCRSwNP
eCRSwNP
Signature score
IL-13 score in fibroblasts
C
CCL26 (ng/mg total protein)
Periostin (ng/mg total protein)
D
Mean expression in group
NK/T Cells
Neutrophils
Myeloid Cells
Mast Cells
Fibroblasts
Epithelial Cells
Endothelial Cells
B Cells
CCL26
Periostin
E
CCL26 in fibroblast culture supernatants (ng/ml)
Periostin in fibroblast culture supernatants (ng/ml)
control
IL-13
OSM
OSM+IL-13
F
CCL26 in HNEC culture supernatants (ng/ml)
Periostin in HNEC culture supernatants (ng/ml)
G
mRNA level in fibroblasts (normalized to GAPDH)
control
OSM
IL4R
IL2RG
IL13RA1
IL13RA2
R = 0.57
p = 0.016
IL4R expression in fibroblasts
OSM expression in CRSwNPs
H
p < 0.0001
R = 0.7216
Elastase in neCRSwNPs (ng/mg total protein)
OSM in neCRSwNPs (ng/mg total protein)
p = 0.0052
R = 0.5221
IL-17A in neCRSwNPs (ng/mg total protein)
p = 0.0378
R = 0.4017
G-CSF in neCRSwNPs (ng/mg total protein)
p = 0.0108
R = 0.4823
IL-6in neCRSwNPs (ng/mg total protein)
p = 0.0092
R = 0.4915
IL-8 in neCRSwNPs (ng/mg total protein)
p = 0.4327
R = 0.1575
IFN-γ in neCRSwNPs (ng/mg total protein)
I
IL-17 score
Epithelial cells
Fibroblasts
CXCL3
CSF3
CXCL6
VNN1
CCL20
SLC26A4
SAA1
SAA2
MTNR1A
TNIP3
CXCL5
HC
eCRSwNP
neCRSwNP
J
Mean expression in group
NK/T Cells
Neutrophils
Myeloid Cells
Mast Cells
Fibroblasts
Epithelial Cells
Endothelial Cells
B Cells
IL-8
G-CSF
K
IL-8 in fibroblast culture supernatants (ng/ml)
G-CSF in fibroblast culture supernatants (pg/ml)
control
IL-17A
OSM
OSM+IL-17A
L
IL-8 in HNEC culture supernatants (ng/ml)
G-CSF in HNEC culture supernatants (pg/ml)